BNL-NUREG--37009

TI86 002509

STRAIN RATE AND TEMPERATURE EFFECTS ON THE STRESS CORROSION CRACKING OF INCONEL 600 STEAM GENERATOR TUBING IN THE PRIMARY WATER CONDITIONS

U. C. Kim and D. van Rooyen
Brookhaven National Laboratory, Bldg. 703
Upton, New York 11973
(516) 282-4050

ABSTRACT

A single heat of Inconel Alloy 600 was examined in this work, using slow strain rate tests (SSRT) in simulated primary water at temperatures of 325°-345°-365°C. The best measure of stress corrosion cracking (SCC) was percent SCC present on the fracture surface. Strain rate did not seem to affect crack growth rate significantly, but there is some question about the accuracy of calculating these values in the absence of a direct indication of when a crack initiates. Demarcation was determined between domains of temperature/strain rate where SCC either did, or did not, occur. Slower extension rates were needed to produce SCC as the temperature was lowered.

INTRODUCTION

It is of obvious importance to preserve the integrity of Inconel Alloy 600 tubing in PWR steam generators so as to prevent loss of primary coolant as well as the escape of radioactivity. SCC related to the presence of high residual or operating stresses has been reported in such tubing, frequently originating on the primary side. Testing performed under conditions where slow plastic deformation continues has been found to be a way of reproducing SCC. In the work reported here, SSRT has been used in order to investigate strain rate and temperature effects on the SCC of a commercial heat of nuclear grade Inconel 600 tubing. The main conclusion is that the SCC response depends on strain rate susceptibility of the material, temperature and environment, and test parameters for investigating alloy 600 cannot be arbitrary. This paper provides information aimed at facilitating the choice of conditions for testing; empirical data are given in detail for one heat of susceptible tubing of Inconel 600 at several strain rates and temperatures.

EXPERIMENTAL

The chemical composition and mechanical properties of our heat of Inconel 600 are listed in Tables 1 and 2. This was a sample of commercially produced, nuclear grade tubing, with 1.7mm wall thickness and 19mm (.75 inch) outside diameter. Longitudinal tensile specimens were fabricated from this tubing, and tested in the curved, as-received shape without flattening. The gauge portion was 12.7mm (.5 inch) long and 2.5mm (0.1 inch) wide. Figure 1 gives the microstructure of the material as revealed by a 8:1 H_2O:H_3PO_4 electrolytic etch and a 5% nital electrolytic etch with a microhardness locating mark. Before testing, the specimens were degreased in acetone, methanol, and rinsed in pure water. The solution chemistry was maintained at 10^{-4}M LiOH and 650 ppm of boron as boric acid with hydrogen overpressure of 0.1 MPa (15 psig) at room temperature. The autoclave was deaerated at room temperature by pressurizing to 3.45 MPa (500 psi) with high purity nitrogen followed by slow depressurization and evacuation; the procedure was repeated five times. Next, the solution volume was reduced by 10 wt.% by steaming at 110°C. A 2.07 MPa (300 psi) overpressure of 5% hydrogen +95% nitrogen was added and the temperature was than raised. The dissolved oxygen was less than 5 ppb after this treatment. Figure 2 shows the experimental set-up for the SSRT specimen. A linear variable differential transformer (LVDT) was used to monitor the specimen extension and a load cell to measure the load. Both of these parameters were continuously recorded during the test.

RESULTS

Strain Rate Effect

Figure 3 shows the stress-strain curves for as-received specimens of Inconel 600 tubing. "A" was obtained in air at room temperature and B to E are the curves at 365°C in the simulated primary water at strain rates of 1.5×10^{-5} sec^{-1}, 3.7×10^{-7} sec^{-1} and 4.2×10^{-8} sec^{-1}, respectively. A correction was made because the specimens were pre-loaded by 200 pounds due to steam pressure on the pull rod at 365°C. Specimen A showed all ductile fracture after test and B showed very little SCC area, i.e. less than 2% of the total fracture surface area

TABLE 1

Chemical Composition of BNL Heat #5 Inconel 600 Tubing

Elements	C	Mn	Al	S	Si	Ni	Cr	Ti	Cu	Fe	Co
Wt.%	.01	.28	-	.006	.08	77.59	15.76	-	.31	7.94	-

TABLE 2

Mechanical Properties of Inconel 600 Tubing

Ultimate Tensile MPa	Yield Strength MPa	Elongation %	Rockwell B Hardness
640	373	44	83.5

after test. Whereas maximum stress of B was 500 MPa (73.5 ksi) and strain at failure time of B was about 50%, maximum stress of E which showed severe intergranular SCC was 300 MPa (44 ksi) and strain at failure time was 18%. During straining, the stress curves of C, D and E deviated from the stress curves of A or B immediately after reaching the yield point.

In order to show the SCC tendency comparatively, the maximum crack penetration was divided by failure time after crack initiation* to give an average crack propagation rate (CPR). Figure 4 shows CPR values at different strain rates for 365°C. CPR at the highest strain rate, 1.5×10^{-6} sec^{-1}, is 2.3×10^{-7} mm sec^{-1}; at a strain rate of 1.4×10^{-7} sec^{-1} it is 2.8×10^{-7} mm sec^{-1} and at the lowest strain rate, 4.2×10^{-8} sec^{-1}, it is 3.3×10^{-7} mm sec^{-1}. When calculated, as presently done, CPR increases only by a factor of 1.5 when the strain rate is decreased from 1.5×10^{-6} sec^{-1} to 4.2×10^{-8} sec^{-1} at 365°C.

Most of the specimens showed irregular crack penetration which makes it difficult to establish an exact crack depth. Consequently, it was found convenient to study the SCC tendency comparatively by measuring area of SCC on the fracture surface, in addition to the CPR studies already described.

*the onset of cracking is estimated and believed to be only approximate, see reference 3.

Figure 5 shows SEM photographs of the fracture surface of the specimen at a strain rate 3.7×10^{-7} sec^{-1}: 5a is the fracture surface of the specimen after test, 5b shows the cracked surface near the inside of the tube after test and other small cracks, while 5c shows the magnified fracture surface of the left top portion of 5a, including a transition region where SCC stopped. Similar SEM photographs were taken of all test pieces after SSRT. The area of SCC was then measured for each fracture surface. Figure 6 shows percentages of SCC and reduction in area. It includes 81% for SCC area at the lowest strain rate (4.2×10^{-8} sec^{-1}) and 2% SCC area at the highest strain rate (1.5×10^{-6} sec^{-1}). These data led to the plotting of a smooth curve of percent SCC area vs. strain rate. Most of the cracked area that consisted of SCC was intergranular at the strain rates 4.2×10^{-8} sec^{-1}, 1.4×10^{-7} sec^{-1} and 3.7×10^{-7} sec^{-1} but the small SCC area of the 1.5×10^{-6} sec^{-1} specimen had different features, and maybe somewhat transgranular at this (highest) strain rate. Percent reduction in area values at 365°C were 16% and 44% at the extremes of the range of strain rates (4.2×10^{-8} sec^{-1} and 1.5×10^{-6} sec^{-1}), respectively.

Temperature Effect

In order to investigate the temperature effect on intergranular SCC, the percent area of SCC obtained at 365°C, 345°C and 325°C was plotted. Figure 7 shows the influence of

temperature on area of SCC at strain rates of 4.2×10^{-8} sec^{-1}, 1.4×10^{-7} sec^{-1}, 3.7×10^{-7} sec^{-1} and 1.5×10^{-6} sec^{-1}. The slope is 1.4×10^{-7} sec^{-1} and the other curves are approximately parallel to this one. From these data, the temperatures which will give 0% area of SCC were extrapolated at the various strain rates, and used to construct Figure 8. As can be seen, it defines the boundary between SCC and dimpled rupture as a function of strain rate and temperature. If, for instance, the strain rate is lower than 2.7×10^{-7} sec^{-1} at 345°C, SCC can be expected.

Figure 9 is an Arrhenius plot of crack propagation against inverse temperature, with a slope corresponding to an activation energy of ca. 44 Kcal/mole. At a strain rate of 4.2×10^{-8} sec^{-1}, the CPR values at 365 and 325°C are 3.3×10^{-7} and 3.2×10^{-8} $mm.sec^{-1}$ respectively, with points for other strain rates in close proximity, (where tests were done). Allowing for the small number of points in the present work, agreement with previous data for activation energy is good.

DISCUSSION

Strain Rate Effect

Figure 10 shows that, within the range examined, the maximum stress reached during SSRT decreases as the strain rate is decreased. This agrees with the work of Parkins et al.[1,2] who showed a minimum in the curve of maximum stress plotted against strain rate, and also defined the strain rate range within which SCC occurred in a Mg-Al alloy exposed in a chromate-chloride solution; above or below the range they defined, the material failed in a normal ductile fashion. The test at our lowest strain rate at 365°C, 4.2×10^{-8} sec^{-1}, shows SCC on 81% of the fracture surface area, i.e. active SCC. Therefore, if the concept of a critical range of strain rates for SCC is related to achieving a critical balance between the rate at which bare metal is created by straining and the rate at which the crack tip repassivates in the wake of a period of rapid electrochemical reaction, then it would be expected that an increase of maximum stress might eventually occur under our experimental conditions at strain rates below the range tested. So far such a point has not been found. However, we did determine maximum strain rates for SCC at several given temperatures.

The work reported by Parkins also indicated a plateau where the crack propagation rate remains essentially constant regardless of strain rate up to a value where a transition occurred from intergranular to transgranular fracture due to ductile fracture. In the present work, we observed that at 365°C the average crack propagation rate is almost independent of strain rate in the range from 4.2×10^{-8} sec^{-1} to 1.5×10^{-6} sec^{-1} at 365°C, i.e. the difference is no more than a factor of 1.5 over almost two orders of magnitude change in strain rate. This appears to be a situation generally similar to that reported by Parkins, except that the lower portion of the curve remains to be established. Furthermore, the entire relationship between strain rate and SCC is obviously highly dependent on temperature.

Some comment has to be made regarding the reliability of the present growth rate calculations. In order to get average crack propagation rates, it was assumed that the crack initiates at some time after the yield point is reached in this environment. It is noteworthy that the stress curves of C, D and E deviate from curves of A or B right after reaching their yield points, Figure 3. Earlier work[5] was done using an extrapolation method for approximately determining the points at which cracks initiated in Inconel 600 specimens at various temperatures. These specimens had been somewhat cold worked (flattened after cutting from split tubes), and they indicated that cracks in pure water, with H_2, first started at about 3.1%, 4.3% and 6.3% strain at 365°C, 345°C and 325°C respectively. The extrapolation was made after examining the crack lengths of many specimens taken out of test at various times of exposure. For the present, these values were used for the crack initiation calculations because no others are available. It is clear, however, that direct determination of crack initiation in each individual test is required for more reliable CPR calculations.

Temperature Effect

As was stated earlier, many specimens showed irregular crack depths after tests, adding some difficulty in determining CPR accurately. Therefore, percent area of SCC was also measured to express the SCC susceptibility. The limiting strain rate above which an all dimpled surface will be observed and below which intergranular SCC surface will be found is strongly dependent on the temperature and has a temperature relationship expressed by the curve in Figure 8. From the extrapolated lower end of this curve to the operating temperature of a cold leg of PWR's, SCC can be predicted if the local deformation rate of the steam generator tubing is lower than about 2×10^{-8} sec^{-1} at 290°C or 5×10^{-8} sec^{-1} at 310°C. It would be interesting to extend this work using cyclic stresses in the same approximate range, so that longer tests can be done without reaching the ultimate strength.

Although our present work concentrated only on variations in temperature and strain rate, it

is believed that a broader, more general conclusion along the same line will apply. In other words, it seems logical that if the susceptibility of Alloy 600 is changed by means other than temperature, e.g. by the processing of the metal or a change in environment, then a similar strain rate dependence will be operative. This may well apply to other alloy systems also.

The activation energy with as-received specimens of the heat used is about 44 Kcal/mole from Figure 9 for growth rates, and it is in reasonably good agreement of the earlier data[5] with flattened BNL specimens of the same heat. However, the CPR magnitude is 3.3×10^{-7} mm sec^{-1} with as-received specimens compared to 9.0×10^{-7} mm sec^{-1} with flattened specimens at 365°C, i.e. a difference of a factor of 2.7 at 365°C. Expected CPR is about 4×10^{-9} mm sec^{-1} at 290°C at a strain rate 4.2×10^{-8} sec^{-1}, using the data above for the calculation, and about 1.5×10^{-8} mm sec^{-1} at 310°C.

CONCLUSIONS

1. There is a strain rate range where the average crack propagation rate is almost independent of strain rate. CPR is increased only by a factor of 1.5 when the strain is decreased from 1.5×10^{-6} sec^{-1} to 4.2×10^{-8} sec^{-1} at 365°C.

2. The area of SCC on the fracture surface is changed from 2% to 81% at 365°C in the strain rate range of about 2×10^{-6} to 4×10^{-8} sec^{-1}.

3. The percent area of SCC and limiting strain rate below which SCC will be shown are strongly dependent on temperature. The limiting strain rate gives a smooth curve in the temperature range of 325 to 365°C when plotting logarithmic limiting strain rate versus temperature. The predicted limiting strain rate is 5×10^{-8} sec^{-1} at 310°C, and 2×10^{-8} sec^{-1} at 290°C for the heat of Inconel used.

4. The activation energy for CPR in the as-received BNL heat of Inconel 600 is about 44 Kcal/mole and it is in reasonably good agreement with earlier data for cold worked specimens. However, the actual magnitude of crack growth rate is lower by the factor of 2.7 at 365°C than the cold worked pieces. The expected CPR is 1.5×10^{-8} mm sec^{-1} at 310°C at a strain rate of 4.2×10^{-8} sec^{-1}, and about 4×10^{-9} mm.sec^{-1} at 290°C.

5. Refinements are needed for greater accuracy in determining CPR, because the onset of SCC must be known for each specimen in order to make a correct calculation.

ACKNOWLEDGMENT

The U. S. Nuclear Regulatory Commission provided partial financial support for this work. The authors also wish to thank T. C. Roberts and J. Barry for their invaluable assistance in operating the test facilities, preparing and examining specimens, as well as R. Sabatini for extensive scanning electron microscope work. One author (U. C. Kim) gratefully acknowledges the Korea Science and Engineering Foundation and Korea Advanced Energy Research Institute for their support during the time spent at BNL as a visiting scientist.

REFERENCES

1. R. N. Parkins, "Development of Strain-Rate Testing and Its Implications," Stress Corrosion Cracking — The Slow Strain Rate Technique, ASTM-STP-665, p. 5, G. M. Urgiansky and J. H. Payer, Eds., 1979.

2. W. R. Wearmouth, G. P. Dean and R. N. Parkins, "Role of Stress in the Stress Corrosion Cracking of a Mg-Al Alloy," Corrosion, Vol. 29, No. 6, pp. 251-258, NACE, 1973.

3. T. S. Bulischeck and D. van Rooyen, "Stress Corrosion Cracking of Alloy 600 Using the Constant Strain Rate Test," Corrosion, Vol. 37, No. 10, pp. 597-607, NACE, 1981.

4. T. S. Bulischeck and D. van Rooyen, "Effect of Environmental Variables on the Stress Corrosion Cracking of Inconel 600 Steam Generator Tubing," Nuclear Technology, Vol. 55, pp. 383-393, ANS, 1981.

5. R. Bandy and D. van Rooyen, "Stress Corrosion Cracking of Inconel 600 in High Temperature Water — an Update," Paper 139, NACE, Corrosion 1983, Anaheim, CA, April 1983, Corrosion, 40, 425 (1984).

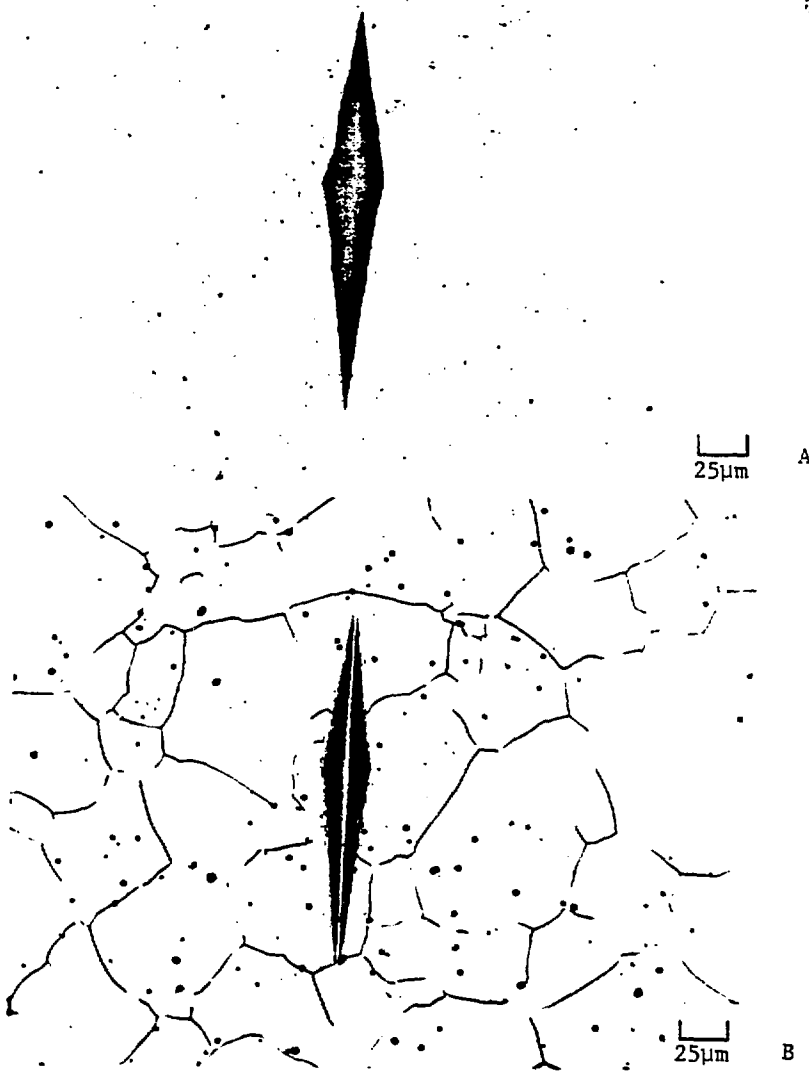

Figure 1 Microstructure of as-received BNL heat #5 Alloy 600 tubing.

a) phosphoric acid etch
b) nital etch

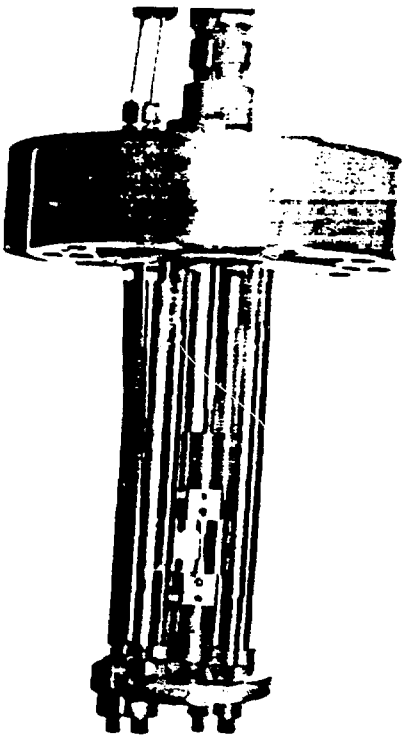

Figure 2 Close-up of the experimental setup for constant extension rate testing.

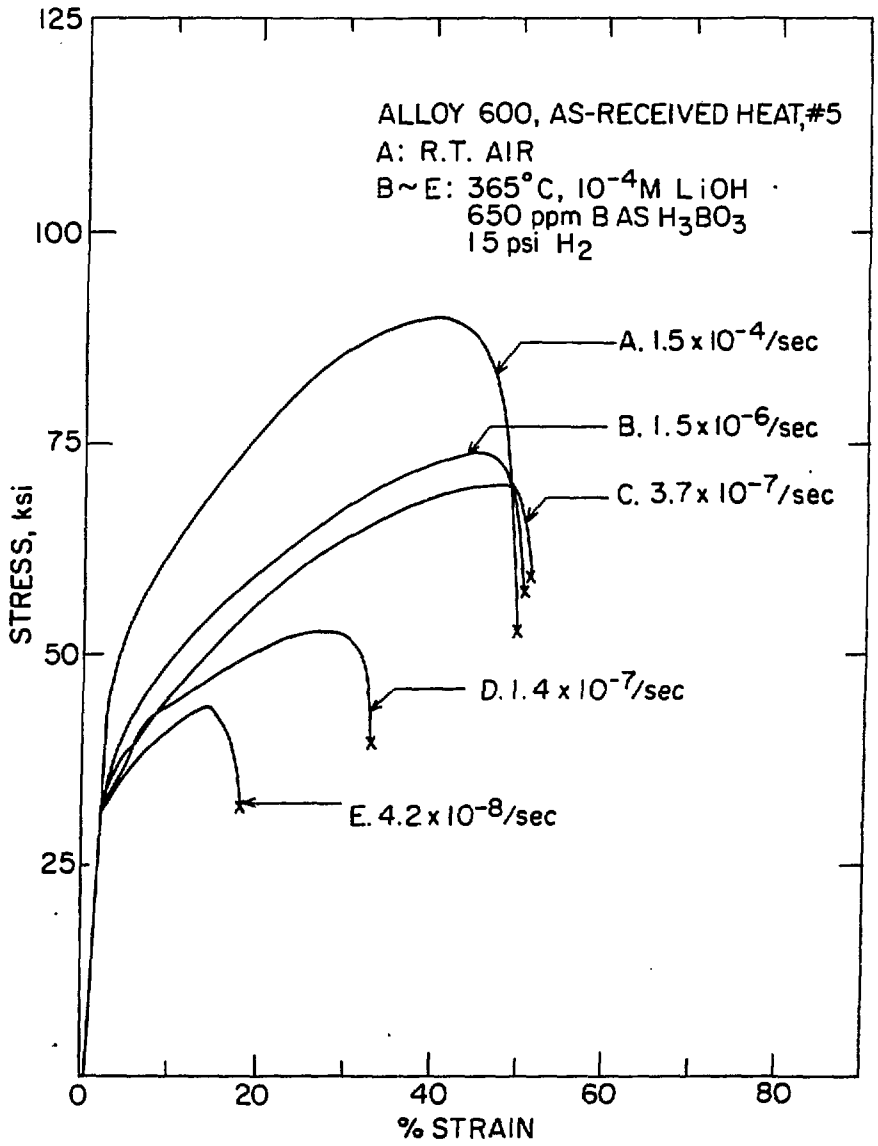

Figure 3 Stress-strain curves for as-received BNL heat #5 Alloy 600 tubing.

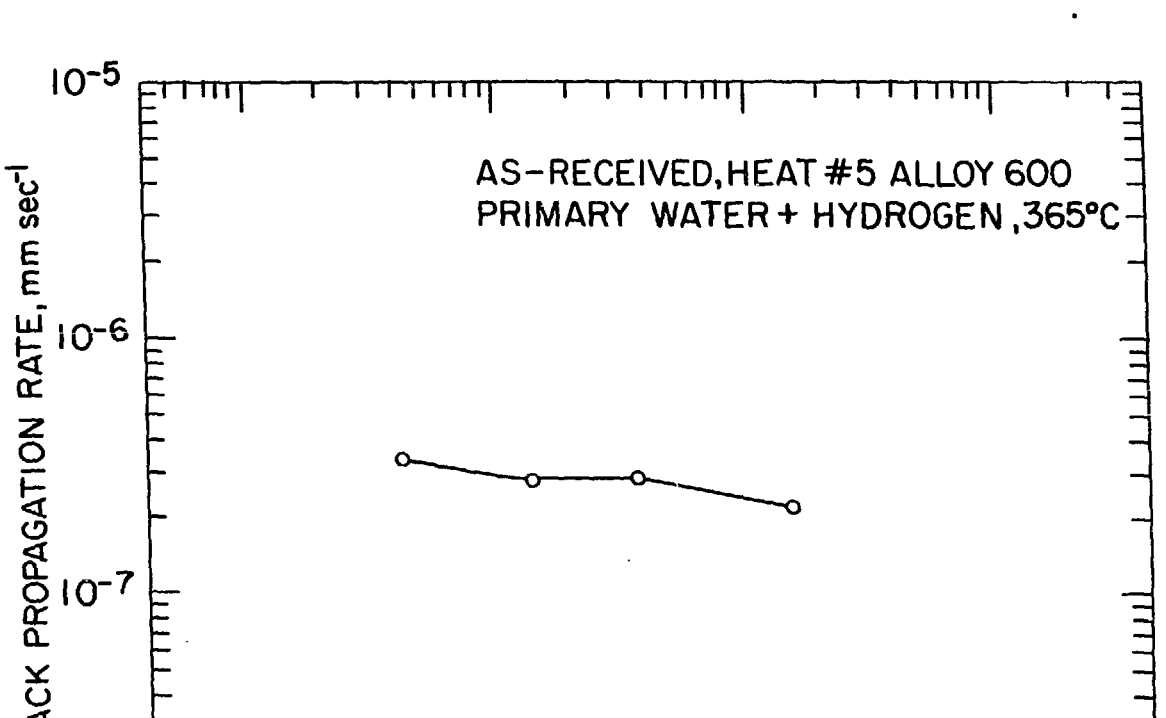

Figure 4 Strain rate effect on average crack propagation rate for BNL heat #5 Alloy 600 tubing.

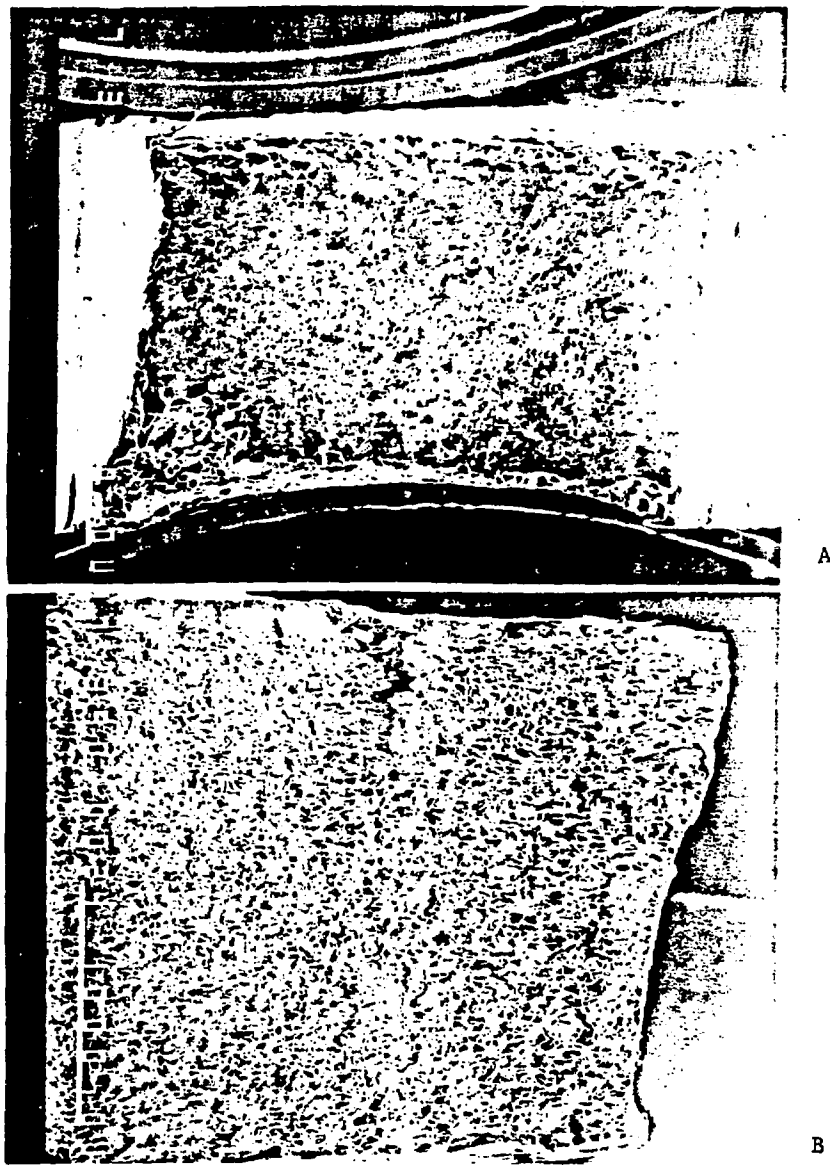

Figure 5 SEM fractograph of the BNL heat #5 Alloy 600 specimen at a strain rate, 3.7×10^{-7} sec^{-1}.

a) fractured surface
b) inside diameter surface

C

Figure 5c Magnified SCC boundary of the left top portion of 5a).

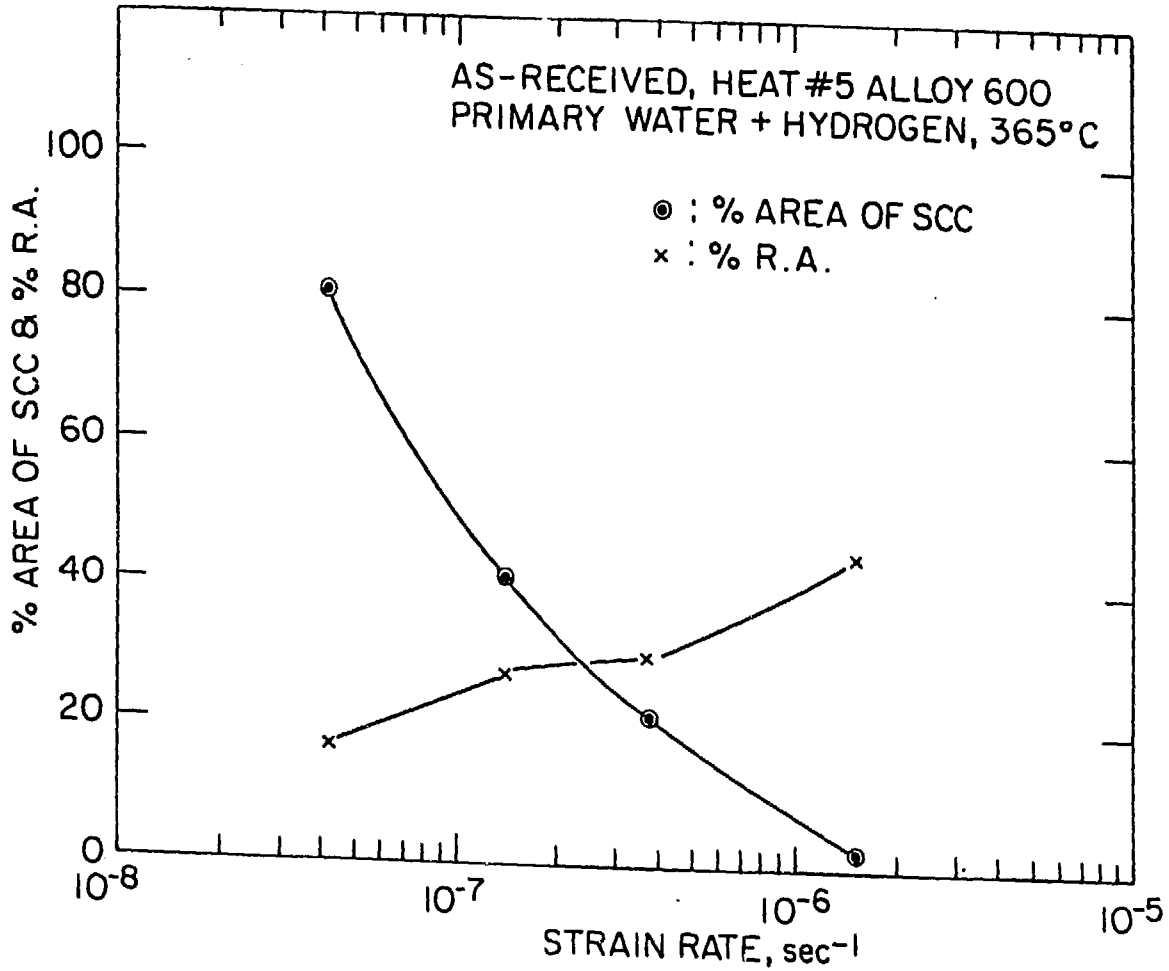

Figure 6 % area of SCC and % reduction area versus strain rate for BNL heat #5 Alloy 600 tubing.

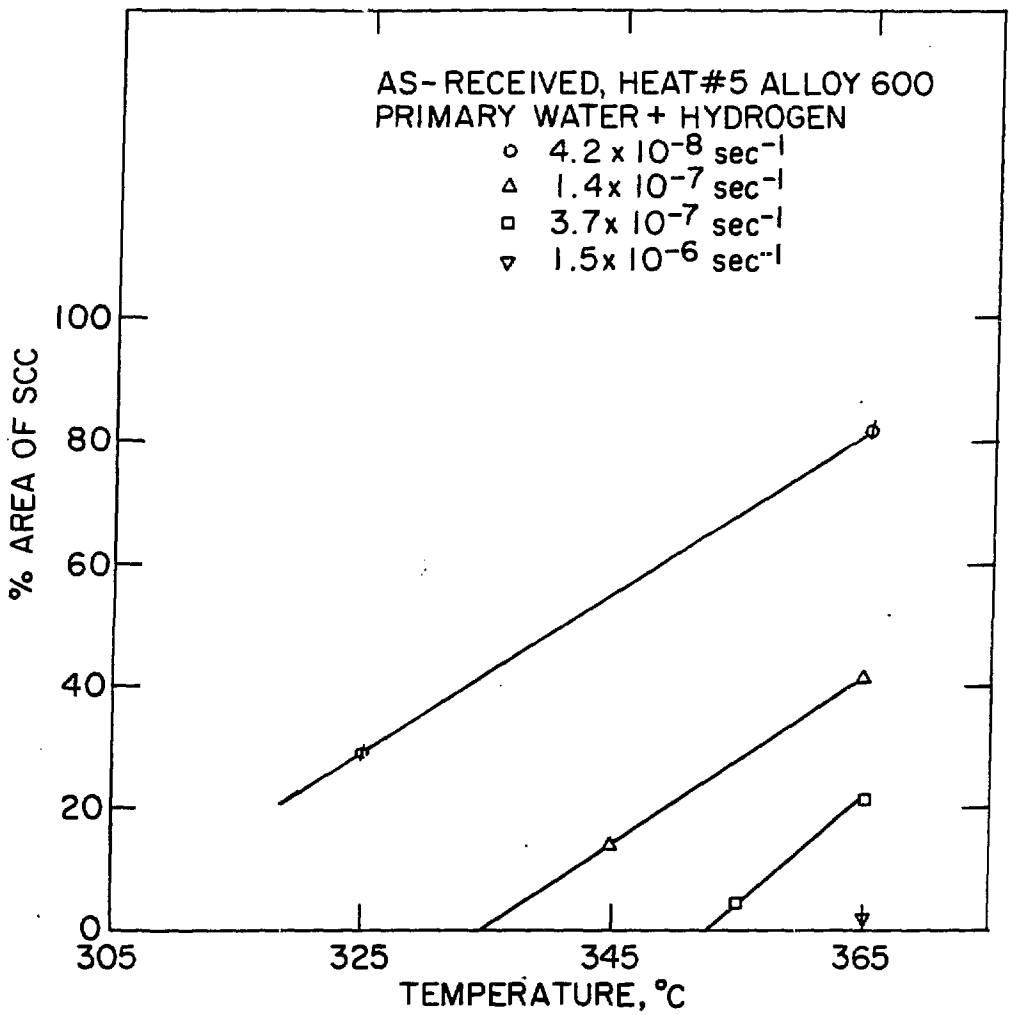

Figure 7 Temperature effect on % area of SCC for BNL heat #5 Alloy 600 tubing at constant strain rates.

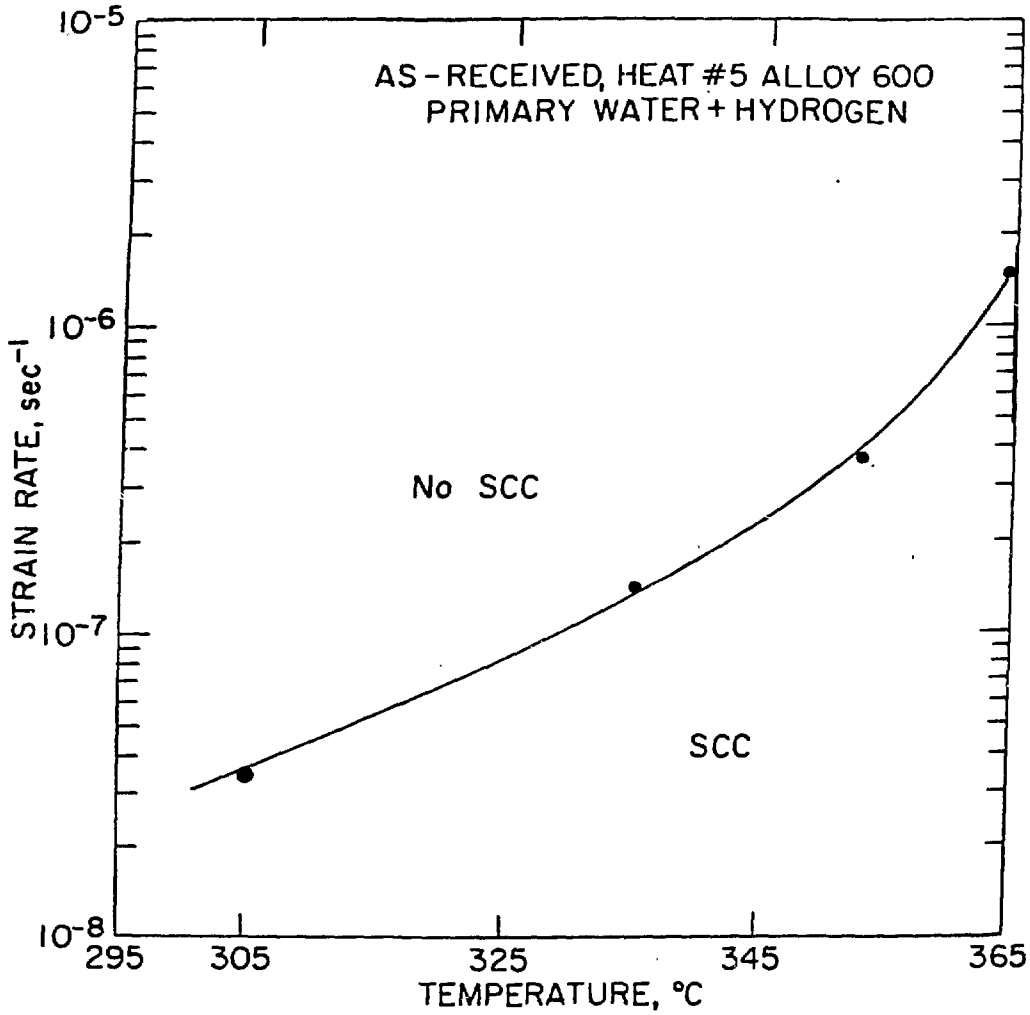

Figure 8 Temperature effect on limiting strain rate below which SCC is observed for BNL heat #5 Alloy 600 tubing.

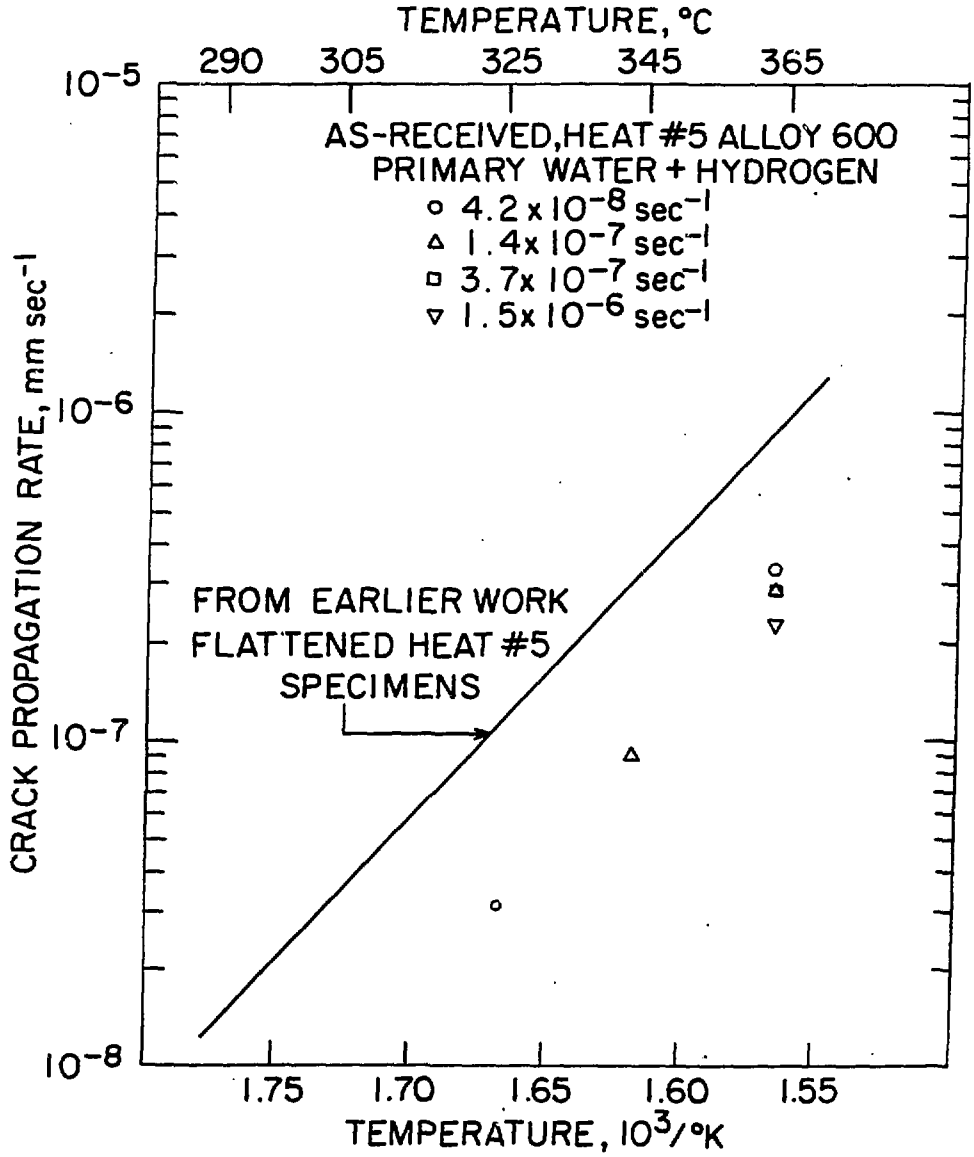

Figure 9 Temperature effect on average crack propagation rate for BNL heat #5 Alloy 600 tubing with and without flattening.

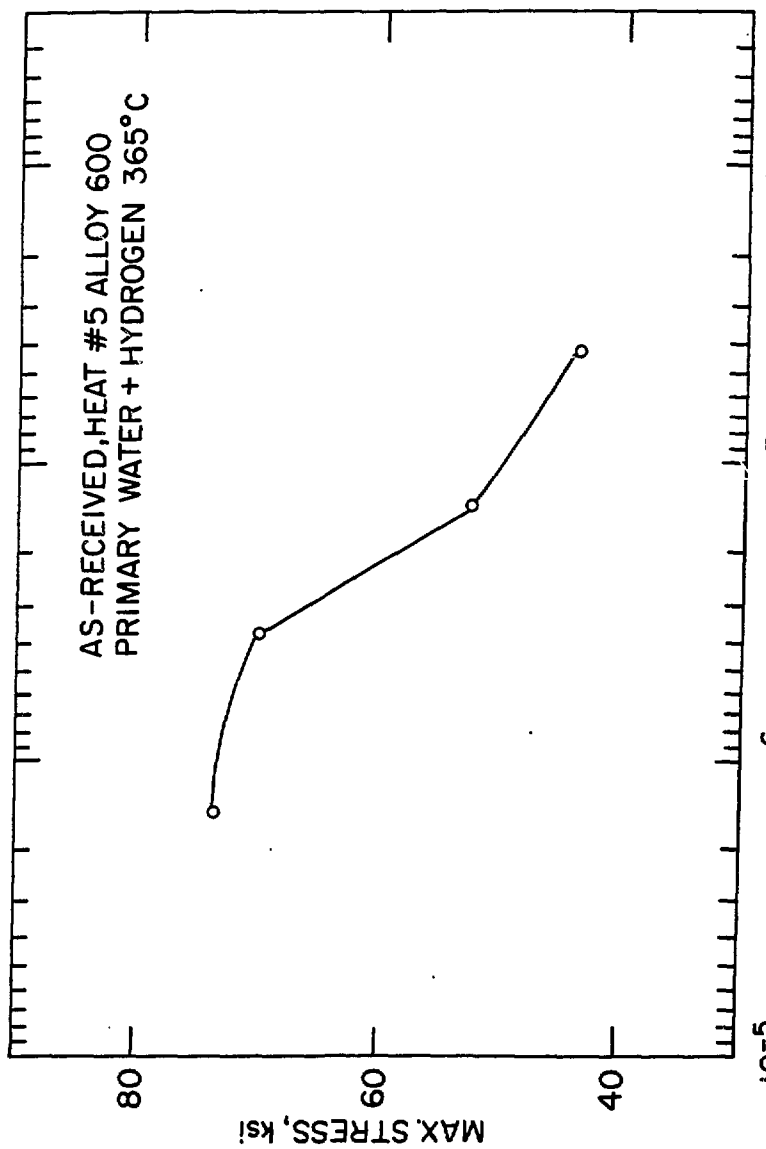

Figure 10 Strain rate effect on maximum stress for BNL heat #5 Alloy 600 tubing.